Spectroscopy of the $5S_{1/2}$ to $6P_{3/2}$ Rb line

Faustmann Christian

Faculty of Physics
Technical University of Vienna

This thesis is submitted for the degree of
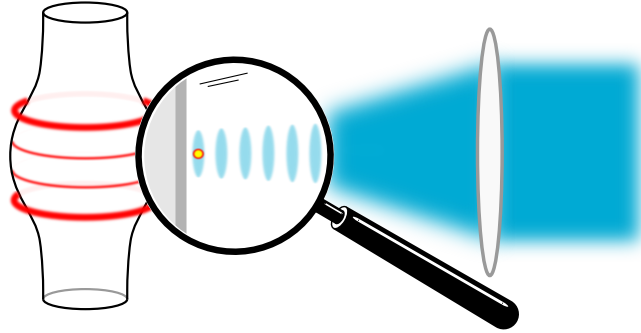*Bachelor of Science*

Introduction

Fig. 1 Schematic representation of a WGM resonator and a optical dipole trap

One of Prof. Rauschenbeutel projects uses a novel type of whispering-gallery-mode (WGM) resonator interfaced via nanowaveguides and coupled to single Rubidium atoms to carry out experiments in the realm of Cavity Quantum Electrodynamics. The WGM resonator is a so-called bottle-microresonator (BMR) manufactured from a standard optical glass fiber in a heat and pull process. The light is radially confined inside the resonator by total internal reflection and propagates along the circumference of the resonator. In such a structure, a signicant fraction of the light field propagates in the evanescent field. By overlapping this field with the evanescent field of an optical nanofiber, light can be coupled into and out of the resonator very efficiently. Due to the extremely low absorption of silica (and low surface roughness) we can produce bottle-resonators with ultra-high optical Q-factor exceeding 10^8. Rubidium atoms are delivered to the resonator using an atomic fountain. When the atoms enter the vicinity of the WGM, and they are in the evanescent field they can be strongly coupled to the light. For the moment the ^{85}Rb atoms are only flying by the resonator for ~2 µs. Moreover the distance between the resonator and the atom is not controlled. This uncertainty induces fluctuations on the atom-resonator coupling from shot to shot and limits the efficiency of the different devices demonstrated with the setup. The short duration of the atom light interaction also prevents the manipulation of the atomic state, necessary for the realization of complex quantum information protocols such as two photon gates [1]. The solution would be to trap the atom at the vicinity of the BMR. The choice made to trap

the atom is to use a dipole trap created from the retroreflection of a focused beam on the resonator surface inspired from [2] (see Fig. 1). Due to the experiment configuration, the trap can not be loaded from a dense cloud, but only from the atoms flying next to the resonator, which have a non-zero velocity, which further implies that a big trap depth is needed. The usual dipole traps are built with lasers detuned from the transition between the ground and the first excited state. But this would create a trap too far from the resonator and thus in this thesis, we discuss the possibility to realise a trap detuned from the second exited state of ^{85}Rb which has transitions at $\lambda \approx 420 \, \text{nm}$. In this thesis, we will also evaluate the parameters needed for such a trap, and then report on an absorption spectroscopy measurement leading to the estimation of the saturation intensity of this $420 \, \text{nm}$ transition.

Table of contents

Chapter 1

Theory of laser trapping of atoms

Atoms can be trapped by a force deriving from the gradient of an optical potential created by the dispersive interaction of the atomic dipole moment with the intensity gradient of the light field. These traps can be used to confine the atoms in 3D and counteract gravity and confine the atoms in 3D. In the case of large detunings the expressions for the dipole potential and scattering rate [3] are the following:

$$U_{\mathrm{dip}}(z) = \frac{3\pi c^2}{2\omega_0^3} \frac{\Gamma}{\Delta} I(z) \;, \tag{1.1}$$

$$\Gamma_{\mathrm{sc}}(z) = \frac{3\pi c^2}{2\hbar\omega_0^3} \left(\frac{\Gamma}{\Delta}\right)^2 I(z) \;. \tag{1.2}$$

Where c is the speed of light, Γ characterizes the coupling rate between the two atomic levels of the atomic transition, Δ is the detuning between the light and the atomic transition ($\Delta = \omega - \omega_0$), where ω is the driving pulsation of the light field, $\omega_0 = 2\pi \frac{c}{\lambda_0} = 2\pi \nu_0$ the atomic transition pulsation and $I(z)$ corresponds to the intensity of the light field at a distance z from the resonator. Dipole traps can be divided into two main classes, red-detuned traps ($\Delta < 0$) and blue-detuned traps ($\Delta > 0$). Below an atomic resonance (red) the dipole potential is negative and the potential

Fig. 1.1 Illustration of dipole traps with red and blue detuning. The grey area represents regions of high intensity.

minima are therefore found at positions of maximum intensity. For a blue-detuned light the potential minima correspond to minima of the intensity and the interaction repels atoms from the field as seen in Fig. 1.1. For our setup we will consider a red-detuned trap.
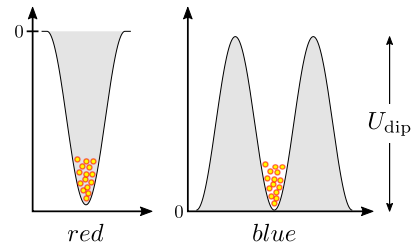
There are three different trap configurations possible:

- *focused-beam trap*: Focused-beam traps are consisting of a single strongly focused beam and have a confinement volume proportional to $z_R \times w_0{}^2$, where z_R is the Rayleigh length and w_0 is the beam waist radius.

- *crossed-beam trap*: A crossed-beam configuration uses two beams of waist w_0 and w_1 which intersect at their foci. The confinement volume reduces to the intersection of the contributing beams, which is in case where w_0 is smaller than w_1: $w_0{}^2 \times w_1$.

- *standing wave trap*: In case of a standing wave trap the atoms are axially confined in the antinodes of a standing wave. If the standing wave is created through a retroreflection the first antinode and therefore first trapping site lies at a distance of $\frac{\lambda}{4}$ from the surface (see Fig. 1.2). The resulting volume is in the order of $w_0{}^2 \times \frac{\lambda}{4}$.

For our experiment it is important that the atoms are as close as possible from the resonator, because the interacting evanescent field in the resonator decreases exponentially with a decay length of $\frac{\lambda_{at}}{2\pi}$ where λ_{at} is the wavelength of the cavity field tuned to the atomic transition. $5S_{1/2} \rightarrow 5P_{3/2}$ (D_2 line of Rb at $780\,\text{nm}$) has a decay length of $124\,\text{nm}$.

If one uses a laser closely detuned from the D_2 line $5S_{1/2} \rightarrow 5P_{3/2}$ to trap the atom, i.e. $783\,\text{nm}$, this leads to a distance of $\frac{\lambda}{4} \approx 190\,\text{nm}$. This would be already too far from the resonator. Interestingly Rubidium atoms also have a transition from $5S_{1/2}$ to $6P_{3/2}$ at $420\,\text{nm}$ as can be seen in Fig. 1.3. In the next section we will establish the trap parameters necessary to trap the atoms.
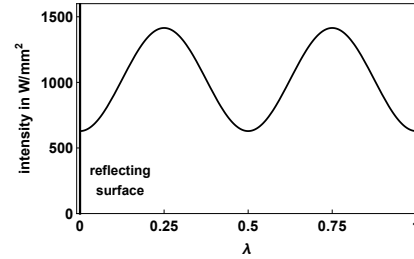

Fig. 1.2 1D Intensity distribution of a retroreflected gaussian laser beam for a partial standing wave with $r = -0.2$.
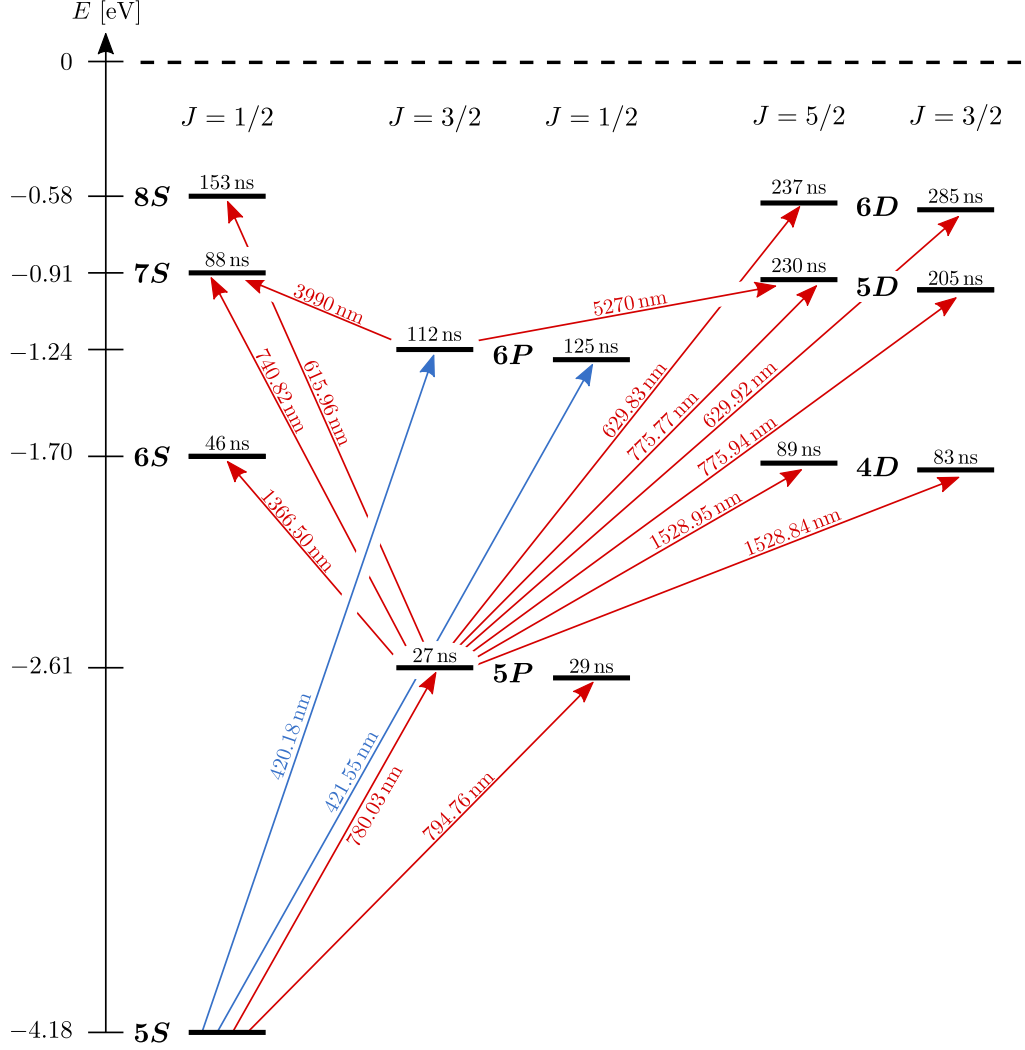
Fig. 1.3 Level scheme of ^{85}Rb with lifetimes and transition wavelength of the first states [4].

As we can see in Eq. (1.1) the dipole potential is proportional to $\frac{I}{\Delta}$, which means that we have two degrees of freedom, the detuning and the power ($I \propto \frac{power}{cross\ section}$). To choose our parameters properly we have to consider some constraints. We want to keep the scattering rate as low as possible, because each photon scattered may depolarize the atom or depump the atom in which case it cannot be detected anymore. The scattering rate is proportional to $\frac{I}{\Delta^2}$ (Eq. 1.2), so a detuning as big as possible would be beneficial. On the other hand laser power is limited ($P_{\max} = 80\,\text{mW}$), due to the maximum power output of our laser. And additionally we do not want to send too much power onto the resonator, because due to the highly focused beam ($w_0 = 3.6\,\mu\text{m}$), the more energetic wavelength and more absorption of the glass in the blue spectrum the resonator could be damaged. To compensate the lower laser power the detuning has to be small. However if Δ

smaller than the separation between the D_1 and D_2 lines (420 & 421 nm) then we need to take the fine structure of the atom into account and equations (1.1) and (1.2) rewrite as [3]

$$U_{\text{dip}}(z) = \frac{\pi c^2}{2\omega_0^3} \left(\frac{2\,\Gamma_{\omega,D2}}{\Delta_{D2}} + \frac{\Gamma_{\omega,D1}}{\Delta_{D1}} \right)\, I(z)\,, \tag{1.3}$$

$$\Gamma_{\text{sc}}(z) = \frac{\pi c^2}{2\hbar\omega_0^3} \left(\frac{2\,\Gamma_{\omega,D2}\,\Gamma_{\omega,D2,tot}}{\Delta_{D2}^2} + \frac{\Gamma_{\omega,D1}\,\Gamma_{\omega,D1,tot}}{\Delta_{D1}^2} \right)\, I(z)\,. \tag{1.4}$$

It should be noted that as $6P_{1/2}$ and $6P_{3/2}$ are not the first excited states, there exist several possible decay channels from there to the ground state. $\Gamma_{\omega,Dx}$ are the transition strengths from $5S_{1/2} \to 6P_{1/2}$ and $5S_{1/2} \to 6P_{3/2}$, while $\Gamma_{\omega,Dx,tot}$ represents the total decay rates of the $6P_{1/2}$ and $6P_{3/2}$ states with $\frac{1}{\Gamma_{\omega,Dx,tot}}$ the mean lifetime of the state given in Fig. 1.3 and Δ_{Dx} represents $\omega - \omega_{0,Dx}$. All values can be found in table 2.1.

It should be noted that $\Gamma_{6P_{3/2}}$ is 20 times weaker than $\Gamma_{5P_{3/2}}$ and thus, for the same trap depth a shorter detuning or higher power will be needed comparatively to a dipole trap around 780 nm.

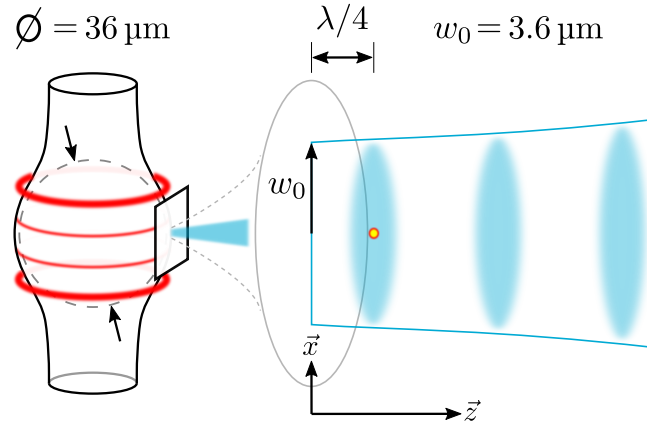## 1.1   Possible configuration of optical dipole trap

Fig. 1.4 Experimental setup and intensity distribution.

To calculate the trap potential we have to derive the intensity of the standing wave. The trap is produced by a beam focused down to at radius of $w_0 = 3.6\,\mu$m. While the resonator diameter is 36 μm (as shown in Fig. 1.4). Thus, one can consider that the beam is retroreflected on a planar surface. With this assumption the electric field becomes:

$$\vec{E}(z) = E_0\, \vec{x}\, \left(e^{-ik_z z} + re^{ik_z z} \right) \tag{1.5}$$

with r the reflection coefficient in amplitude, which is in case of a glass/vacuum interface $r = -0.2$. k_z is the wave vector in z-direction and equal to $\frac{2\pi}{\lambda}$. This leads to the intensity

$$I(z) = \frac{2|\vec{E}(z)|^2}{\eta} \tag{1.6}$$

depicted in Fig. 1.2. Where $\eta = \eta_0 = \frac{1}{\epsilon_0 c_0} \approx 377\,\Omega$ is the characteristic impedance of free space and $\frac{2\,E_0{}^2}{\eta}$ will be denoted as the maximum intensity I_0 and related to the power of a gaussian beam as

$$P_0 = \frac{1}{2}\,I_0 w_0{}^2 \pi \ . \tag{1.7}$$

The range of power accessible is between $0 \ < \ P_0 \ < 80\,\mathrm{mW}$, due the maximum laser output power.

The trap depth must be bigger than the energy of the atom, here the kinetic energy $E_{kin} = \frac{1}{2}m_{Rb}v^2$ has to be taken into account due to the fact that the atoms are free falling for up to $60\,\mathrm{ms}$. It corresponds in terms of temperature to $E_{kin}/k_B = 1.77\,\mathrm{mK}$. Our trap is conservative. When an atom is captured it gains the potential energy at its position $E_{pot}(z)$ and if $E_{kin} + E_{pot}(z)$ is greater than $E_{pot,\mathrm{max}}$ then the atom will not be trapped. Therefore one should add a safety margin to capture more atoms. For example a $5\,\mathrm{mK}$ trap would capture $\frac{5-1.77}{5} \approx 60\,\%$ of atoms entering the trap if all the atoms have the maximum kinetic energy (worst case scenario). In our setup we are so close to the resonator that the atoms are also sensitive to the Van-der-Waals potential[5]

$$U_{VdW} = -\frac{C_3}{r^3}\ . \tag{1.8}$$

The C_3 coefficient is $h \cdot 770 \cdot 10^{-18}\,\mathrm{Hz\,m}^3$ [6], where h is Plank's constant.

Fig. 1.5 Overlap of dipole and Van-der-Waals potential.

Fig. 1.6 Trap depth for different detuning.

The total potential seen by the atoms is $U_{VdW} + U_{dip}$ (see Fig. 1.5). The depth of the potential well is now the difference between the reduced first maximum and the first minimum at $\lambda/4$ (see Fig. 1.7). For our trap we expect to have $20\,\mathrm{mW}$ of laser power accessible. The power loss include locking the laser to a fixed frequency ($5\,\mathrm{mW}$), because the frequency deviation in free running can be on the order of $1\,\mathrm{GHz}$ when we need to be only $10\,\mathrm{GHz}$ from resonance away (see. Fig. 1.6). One also needs to take into account the losses due to
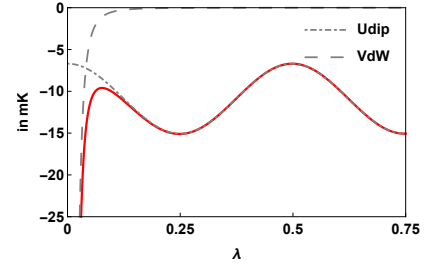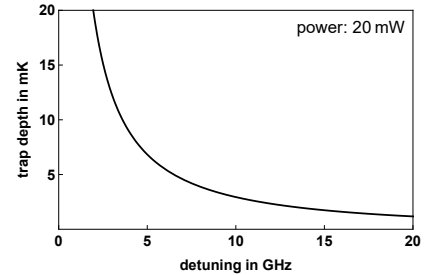
the optical path of the beam before reaching the atoms, which will contain acousto-optical modulators and fiber coupling. As we can see in Fig. 1.6 for $20\,\mathrm{mW}$ power the detuning has to be lower than $7\,\mathrm{GHz}$. For a detuning of $6\,\mathrm{GHz}$ we get a trap depth of $5.5\,\mathrm{mK}$ as shown in Fig. 1.7.

In order to set the laser detuning properly, we need to realize a spectroscopy on the $5S_{1/2} \to 6P_{3/2}$ transition (see Chapter 3).

As seen in equation 1.3 to calculate the trap depth, the transition strength plays a significant role. As $\Gamma_{6P_{3/2}}$ is harder to determine, but can be linked to the saturation intensity by the theoretical formula

Fig. 1.7 Calculated trap potential for $20\,\mathrm{mW}$ power and a $6\,\mathrm{GHz}$ detuning.

$$I_{s,420} = \frac{\Gamma_{\omega,tot,420}{}^2 \cdot \omega_{420}{}^3 \cdot I_{s,780}}{\Gamma_{\omega,420} \cdot \Gamma_{\omega,780} \cdot \omega_{780}{}^3} \quad = 126\,\mathrm{W\,m^{-2}}\;,$$
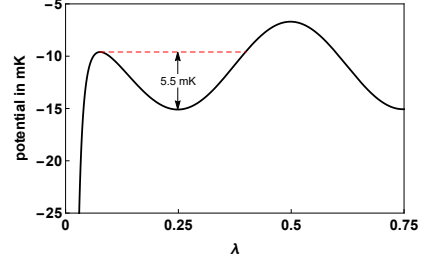
$$(1.9)$$

which we would like to confirm. The index 420 corresponds to $5S_{1/2} \to 6P_{3/2}$ and the index 780 to $5S_{1/2} \to 5P_{3/2}$. In the next chapter we will discuss how we can make use of the light matter interaction to measure I_s by realising an absorption spectroscopy measurement.

Chapter 2

Absorption of photon by an atom

The purpose of this section is to outline the basic features observed in saturated absorption spectroscopy and relate them to simple atomic and laser physics principles. For this we will follow the guidance of [7] and [8].

Electrons can orbit around the atom nucleus following different trajectories which are quantified, the so called orbitals. It is energetically preferable that the electron orbit around the atomic nucleus in the lowest possible orbitals, but it is possible to excite the electron in different higher excited states. The difference of energy states are in the range of typically optical frequencies, which give rise to absorption spectrum. The atomic transitions are sufficiently separated such that, when probing close to one resonance, one can consider that they behave as a 2 level system.

2.1 Laser interactions - Two-level atom

We begin with the interaction between a laser field and a sample of stationary atoms having only two possible energy levels. Aspects of thermal motion will be treated subsequently. The ground state is denoted $|g\rangle$ of energy E_0 and the excited state $|e\rangle$ of energy E_1. The transition frequency ν_0 is given by Planck's law

$$h\nu_0 = E_1 - E_0 \ . \tag{2.1}$$

For the considered transition, ν_0 is in the optical domain. There can three transition processes happen, as described in Fig. 2.1:
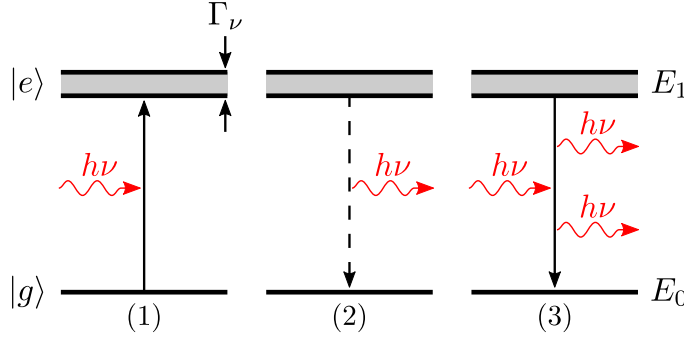
Fig. 2.1 Two-level atom model

(1) *absorption*: Atom in the ground state absorbs a photon with the energy $h\nu_0$ and is excited. The absorption process is described by a transition rate or probability per unit time and is proportional to the laser intensity I (SI units of $\mathrm{W\,m^{-2}}$) and is only significantly different from zero when the laser frequency ν is near the resonance frequency ν_0 of the transition. This transition rate will be denoted $\alpha\,I$, where

$$\alpha = \alpha_0\,\mathcal{L}(\nu,\nu_0) \qquad (2.2)$$

and

$$\mathcal{L}(\nu,\nu_0) = \frac{1}{1 + 4\,(\nu-\nu_0)^2/\Gamma_\nu{}^2} \qquad (2.3)$$
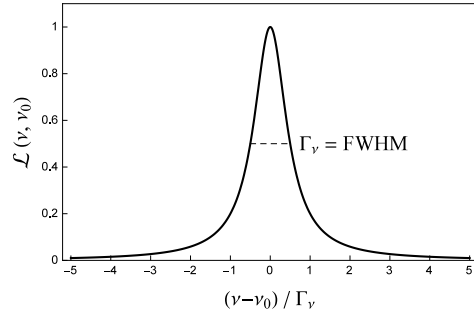

Fig. 2.2 The Lorentzian line shape profile for a transition

gives the *Lorentzian* frequency dependence with a full width at half maximum (FWHM) or *natural linewidth* Γ_ν of this transition as shown in Fig. 2.2. The maximum transition rate $\alpha_0\,I$ occurs right on resonance ($\nu = \nu_0$).

Another important value is

$$I_s = \frac{\Gamma_\omega}{\alpha_0} \qquad (2.4)$$

which defines the saturation intensity of an atom and a specific state. Its significance is that when the laser intensity is equal to the saturation intensity, excited state atoms are equally likely to decay by stimulated emission or by spontaneous emission.

(2) *spontaneous emission*: In the absence of an external field, any initial population of excited state atoms will decay exponentially to the ground state with a mean lifetime Δt.

In the rest frame of the atom, spontaneous photons are emitted in arbitrary directions and polarization with an energy spectrum having a mean $E = h\nu_0$ and a FWHM ΔE given by the Heisenberg uncertainty principle $\Delta E\, \Delta t = \hbar$ or $\Delta E = \Gamma_\omega \hbar$ with the transition rate $\Gamma_\omega = \frac{1}{\Delta t}$. The transition rate corresponds to the *natural linewidth* of the transition

$$\Gamma_\nu = \frac{\Gamma_\omega}{2\pi} \tag{2.5}$$

(3) *stimulated emission*: If a photon of $h\nu_0$ impinges on an atom in the excited state, the atom will de-excite by emitting a photon which has the same characteristics ($\vec{k}$, phase, polarization) as the incident photon. The process of stimulated emission is also described by the same transition rate $\alpha\, I$ as absorption, because the photon emitted or absorbed corresponds to the same transition line.

2.2   The $5S_{1/2} \to 6P_{3/2}$ transition of ^{85}Rb

We want to probe the $5S_{1/2} \to 6P_{3/2}$ transition, which is not the lowest energy transition. Thus when the atom is in the $6P_{3/2}$ state it has several decay channels (e.g. $6P_{3/2} \to 6S_{1/2} \to 5P_{3/2} \to 5S_{1/2}$). Therefore the lifetime of the state $\Delta t = 112\,\text{ns} = \frac{1}{\Gamma_{tot}} \neq \frac{1}{\Gamma_\omega}$. So the transition rate of spontaneous emission differs from absorption and stimulated emission, which are still Γ_ω because they correspond to the single transition at λ_0. For the used $D2$ line at $\lambda_0 = 420\,\text{nm}$ the transition rate $\Gamma_{\omega,D2} = 2\pi \times 0.282\,\text{MHz}$.

2.3   Laser absorption spectroscopy

The arrangement for ordinary laser absorption spectroscopy through a gaseous sample is shown in Fig. 2.3. A laser beam passes through the vapor cell and its intensity is measured by a photodiode detector as the laser frequency ν is scanned through the resonance frequency of an atomic transition.

Fig. 2.3 Basic arrangement for ordinary laser absorption spectroscopy.

To understand the absorption spectroscopy signal we will establish the basic equation describing how the laser intensity changes as it propagates through the sample.
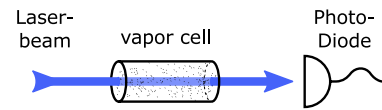
2.4   Equation

When a laser beam propagates through a gaseous sample only absorption and stimulated emission change the intensity I of the laser beam and at the same time affect the proportion of the atoms in the ground P_0 and exited state P_1. Therefore the intensity at $x + \mathrm{d}x$ equals the intensity at x reduced by the missing intensity due to absorption and increased by the intensity due to stimulated emission. Each time there is an absorption process the atom absorbs the energy $h\nu$ from the beam. The rate of absorption is defined by αI, so the power dissipated by one atom is $\alpha I \cdot h\nu$. The number N of interacting atoms with the beam is the atom density n_0 multiplied by the considered volume $V = A \cdot \mathrm{d}x$ where A is the beam cross section. Only the proportion of atoms in the ground state can contribute to the decrease in intensity, so the dissipated power by absorption is

$$\alpha \ I(x) \ h\nu \ n_0 \ A \ \mathrm{d}x \ P_0 \tag{2.6}$$

where P_0 is the proportion of atoms in the ground state. With the definition of *intensity* $= \frac{power}{area}$ one obtains the dissipated intensity by absorption

$$\alpha \ I(x) \ h\nu \ n_0 \ P_0 \ \mathrm{d}x \ . \tag{2.7}$$

Similarly for the stimulated emission the produced intensity is

$$\alpha \ I(x) \ h\nu \ n_0 \ P_1 \ \mathrm{d}x \ , \tag{2.8}$$

where P_1 is the proportion of atoms in the excited state and $P_0 + P_1 = 1$. The variation of the laser intensity from x to $x + \mathrm{d}x$ in the sample is as follows:

$$I(x + \mathrm{d}x) - I(x) = -\alpha \ I(x) \ h\nu \ n_0 \ (P_0 - P_1) \ \mathrm{d}x \tag{2.9}$$

This leads to the differential equation

$$\frac{\mathrm{d}I}{\mathrm{d}x} = -\kappa \ I \tag{2.10}$$

where the *absorption coefficient* (fractional absorption per unit of length)

$$\kappa = \alpha \ h\nu \ n_0 \ (P_0 - P_1) \tag{2.11}$$

It should be noted that the proportionality to $P_0 - P_1$ arises from the competition between stimulated emission and absorption and it is important to appreciate the consequences. If there are equal numbers of atoms in the ground and excited state $(P_0 - P_1 = 0)$, laser photons are as likely to be emitted by an atom in the excited state as they are to be absorbed by

an atom in the ground state and there will be no attenuation of the incident beam. The attenuation maximizes when all atoms are in the ground state ($P_0 - P_1 = 1$) because only absorption is possible. And the attenuation can even reverse sign (become an amplification as it does in laser gain media) if there are more atoms in the excited state ($P_0 > P_1$).

2.5   Doppler shifts

Atoms in a vapor cell move randomly in all three directions with a velocity distribution dependent on the temperature. Only the component of velocity parallel to the laser beam direction will be important when taking into account Doppler shifts and it is this component we refer to with the symbol v. The density of atoms dn in having a velocity comprised between v and $v + dv$ is given by the Boltzmann velocity distribution:

$$dn = n_0 \ \sqrt{\frac{m}{2\pi \ k_B T}} \ \exp\left(-\frac{m \ v^2}{2 \ k_B T}\right) \ dv \qquad (2.12)$$

defining the standard deviation

$$\sigma_v = \sqrt{\frac{k_B T}{m}} \qquad (2.13)$$

It can be rewritten using the canonical form of a Gaussian distribution

$$dn = n_0 \ \frac{1}{\sqrt{2\pi} \ \sigma_v} \ \exp\left(-\frac{v^2}{2 \ \sigma_v^2}\right) \ dv \qquad (2.14)$$

with a mean of zero – indicating the atoms are equally likely to be going in the positive or negative z direction, i.e. they have positive or negative velocities. It is properly normalized so that the integral over all velocities ($-\infty \to \infty$) is n_0, the overall atom density.

Atoms moving with a velocity v see the laser beam Doppler shifted by the amount $\nu \ \frac{v}{c}$. This corresponds to a Doppler shifted resonance frequency

$$\nu_0' = \nu_0 \left(1 + \frac{v}{c}\right) \qquad (2.15)$$

in the lab frame. The sign has been chosen for a laser beam propagating in the positive direction so that the resonance frequency is blue shifted to higher frequencies if v is positive and red shifted if v is negative.

The absorption coefficient $d\kappa$ from a velocity group dn at a laser frequency ν is then obtained from Eq. 2.11 by substituting dn for n_0 and by adjusting the Lorentzian dependence of α so

that it is centered on the Doppler shifted resonance frequency ν_0' (Eq. 2.15).

$$d\kappa = \alpha_0 \ h\nu \ (P_0 - P_1) \ \mathcal{L}(\nu, \nu_0') \ dn \tag{2.16}$$

The absorption coefficient from all atoms is then found by integrating over all velocity classes.

2.6   Absorption coefficient - weak field

We consider the weak-laser intensity case, where we have a very low intensity compared to I_s and therefore nearly all atoms will be in the ground state, i.e., $P_0 - P_1 = 1$ so that

$$d\kappa = \alpha_0 \ h\nu \ n_0 \ \frac{1}{\sqrt{2\pi} \ \sigma_v} \ \mathcal{L}(\nu, \nu_0') \ \exp\left(-\frac{v^2}{2\sigma_v{}^2}\right) \ dv \tag{2.17}$$

and

$$\kappa = \underbrace{\alpha_0 \ h\nu \ n_0 \ \frac{1}{\sqrt{2\pi}\sigma_v}}_{\beta} \int_{-\infty}^{\infty} \frac{1}{1 + 4 \left[\nu - \nu_0 \left(1 + \frac{v}{c}\right)\right]^2/\Gamma_\nu{}^2} \ \exp\left(-\frac{v^2}{2 \ \sigma_v{}^2}\right) \ dv \tag{2.18}$$

After the variable transformation

$$\left| \begin{array}{c} \nu_0' = \nu_0 \left(1 + \frac{v}{c}\right) \\ v = \left(\frac{\nu_0'}{\nu_0} - 1\right) c \\ dv = \frac{c}{\nu_0} \ d\nu_0' \end{array} \right| = \beta \ \frac{c}{\nu_0} \int_{-\infty}^{\infty} \frac{1}{1 + 4 \ (\nu - \nu_0')^2/\Gamma_\nu{}^2} \ \exp\left(-\frac{(\nu_0' - \nu_0)^2 \ c^2}{2 \ \nu_0{}^2 \ \sigma_v{}^2}\right) \ d\nu_0'$$

and substitution $\sigma_\nu = \frac{\nu_0}{c} \ \sigma_v$ we get

$$\kappa = \beta \ \frac{c}{\nu_0} \int_{-\infty}^{\infty} \frac{1}{1 + 4 \ (\nu - \nu_0')^2/\Gamma_\nu{}^2} \ \exp\left(-\frac{(\nu_0' - \nu_0)^2}{2 \ \sigma_\nu{}^2}\right) \ d\nu_0' \tag{2.19}$$

Now we compare the width parameters from the Lorentzian (see table 2.1) with the Gaussian function and at room temperature ($20\,°\mathrm{C}$) (see Fig. 2.4):

$$\sigma_\nu = \frac{c}{\lambda_{\text{D2}}} \sqrt{\frac{k_B T}{m_{Rb85} \, c^2}} \approx 403 \, \text{MHz}$$

$$\Gamma_{\nu,\text{D2}} = 0.282 \, \text{MHz}$$

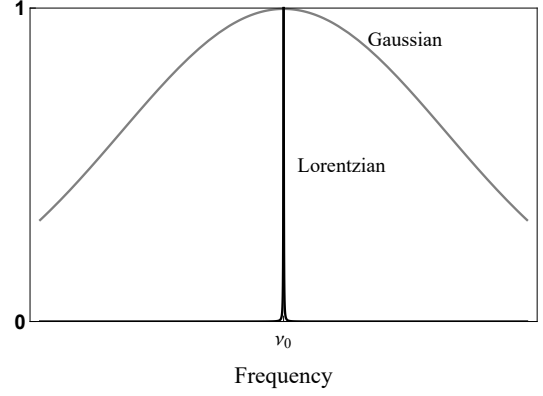$$\Rightarrow \Gamma_{\nu,\text{D2}} \ll \sigma_\nu$$

Fig. 2.4 The Lorentzian compared to the Gaussian profile

As we can see the Lorentzian function is significantly different from zero only within a very narrow range. Consequently the Gaussian remains relatively constant over the width of $\Gamma_{\nu,\text{D2}}$. Therefore Eq. (2.19) can be accurately determined as the integral of the Lorentzian times the value of the exponential at $\nu'_0 = \nu$:

$$= \beta \, \frac{c}{\nu_0} \, \exp\left(-\frac{(\nu - \nu_0)^2}{2 \, \sigma_\nu^2}\right) \int\limits_{-\infty}^{\infty} \frac{1}{1 + 4 \, (\nu - \nu'_0)^2 / \Gamma_\nu^2} \, \mathrm{d}\nu'_0 \tag{2.20}$$

and with the solution of the Lorentzian integral

$$\int\limits_{-\infty}^{\infty} \mathcal{L}(\nu, \nu'_0) \, \mathrm{d}\nu'_0 = \frac{\pi \, \Gamma_\nu}{2} \tag{2.21}$$

we finally get the absorption coefficient in a weak field

$$\kappa = \kappa_0 \, \exp\left(-\frac{(\nu - \nu_0)^2}{2 \, \sigma_\nu^2}\right) \quad \text{with} \quad \kappa_0 = \alpha_0 \, h\nu \, n_0 \, \frac{1}{\sqrt{2\pi} \, \sigma_\nu} \, \frac{\pi \, \Gamma_\nu}{2} \tag{2.22}$$

2.7 Population

To determine the general case of the absorption coefficient we need to determine $P_0 - P_1$. For that we have to take into account the changes to the ground and excited state populations arising from a laser beam propagating through the cell. The rate equations for the ground and excited state are therefore:

$$\frac{\mathrm{d}P_0}{\mathrm{d}t} = \Gamma_{\omega,tot} P_1 - \alpha \, I(P_0 - P_1)$$
$$\frac{\mathrm{d}P_1}{\mathrm{d}t} = -\Gamma_{\omega,tot} P_1 + \alpha \, I(P_0 - P_1) \tag{2.23}$$

where the first term on the right in each equation arises from spontaneous emission and the second term arises from absorption and stimulated emission.

With the additional equation $P_0 + P_1 = 1$ and the steady state condition

$$\frac{\mathrm{d}P_0}{\mathrm{d}t} = \frac{\mathrm{d}P_1}{\mathrm{d}t} = 0 \tag{2.24}$$

we get for the populations

$$P_0 = \frac{\Gamma_{\omega,tot} + \alpha\ I}{\Gamma_{\omega,tot} + 2\alpha\ I}\ ; \qquad P_1 = \frac{\alpha\ I}{\Gamma_{\omega,tot} + 2\alpha\ I} \tag{2.25}$$

which leads to

$$(P_0 - P_1) = \frac{\Gamma_{\omega,tot}}{\Gamma_{\omega,tot} + 2\alpha\ I} \tag{2.26}$$

As we can see the population difference is dependent on $\Gamma_{\omega,tot}$ (spontaneous decay rate), which is related to the *Lorentzian width parameter*. To combine the Lorentzians in α (Eq. 2.2) and $(P_0 - P_1)$ we will define $\Delta\nu = 2\ (\nu - \nu_0)$:

$$\alpha = \alpha_0\ \frac{1}{1 + \Delta\nu^2/\Gamma_\nu{}^2} = \alpha_0\ \frac{\Gamma_\nu^2}{\Gamma_\nu^2 + \Delta\nu^2}\ ; \qquad (P_0 - P_1) = \frac{2\pi\ \Gamma_{\nu,tot}}{2\pi\ \Gamma_{\nu,tot} + 2\alpha\ I} \tag{2.27}$$

and get

$$(P_0 - P_1)\alpha = \frac{2\pi\ \Gamma_{\nu,tot}}{2\pi\ \Gamma_{\nu,tot} + 2I\ \alpha_0\ \frac{\Gamma_\nu^2}{\Gamma_\nu^2 + \Delta\nu^2}}\ \alpha_0\ \frac{\Gamma_\nu^2}{\Gamma_\nu^2 + \Delta\nu^2} = \frac{\alpha_0\ \pi\ \Gamma_\nu^2\ \Gamma_{\nu,tot}}{\pi\ \Gamma_{\nu,tot}\ (\Gamma_\nu^2 + \Delta\nu^2) + I\ \alpha_0\ \Gamma_\nu^2} \tag{2.28}$$

dividing with $\pi\ \Gamma_\nu$ and substitute in the denominator α_0 with the definition of Eq. (2.5) and (2.4) leads to

$$(P_0 - P_1)\alpha = \alpha_0\ \frac{1}{1 + \frac{\Delta\nu^2}{\Gamma_\nu} + \frac{2I}{I_s}\ \frac{\Gamma_\nu}{\Gamma_{\nu,tot}}} = \frac{\alpha_0}{\left(1 + \frac{2I}{I_s}\ \frac{\Gamma_\nu}{\Gamma_{\nu,tot}}\right)}\ \frac{1}{1 + \frac{\Delta\nu^2}{\Gamma_\nu^2\left(1 + \frac{2I}{I_s}\ \frac{\Gamma_\nu}{\Gamma_{\nu,tot}}\right)}} \tag{2.29}$$

and with the definition of the power-broadened *width parameter*

$$\Gamma'_\nu = \Gamma_\nu\sqrt{1 + \frac{2I}{I_s}\ \frac{\Gamma_\nu}{\Gamma_{\nu,tot}}} \tag{2.30}$$

we obtain

$$(P_0 - P_1)\alpha = \frac{\alpha_0}{\left(1 + \frac{2I}{I_s}\ \frac{\Gamma_\nu}{\Gamma_{\nu,tot}}\right)}\ \mathcal{L}'(\nu,\nu_0)\ \text{ and }\ \mathcal{L}'(\nu,\nu_0) = \frac{1}{1 + \frac{4\ (\nu-\nu_0)^2}{\Gamma'_\nu{}^2}} \tag{2.31}$$

2.8   Absorption coefficient - general case

For the general case we take now into account the velocity groups and their corresponding Doppler shifts for the case $P_0 - P_1 \neq 1$ and therefore

$$\mathrm{d}\kappa = h\nu \; n_0 \; \frac{\alpha_0}{(1 + \frac{2I}{I_s} \frac{\Gamma_\nu}{\Gamma_{\nu,tot}})} \frac{1}{\sqrt{2\pi} \; \sigma_v} \mathcal{L}'(\nu, \nu_0') \exp\left(-\frac{v^2}{2 \; \sigma_v{}^2}\right) \mathrm{d}v \tag{2.32}$$

and

$$\kappa = h\nu \; n_0 \; \frac{\alpha_0}{(1 + \frac{2I}{I_s} \frac{\Gamma_\nu}{\Gamma_{\nu,tot}})} \; \frac{1}{\sqrt{2\pi} \; \sigma_v} \int_{-\infty}^{\infty} \frac{1}{1 + 4 \left[\nu - \nu_0 \left(1 + \frac{v}{c}\right)\right]^2/\Gamma_\nu'{}^2} \exp\left(-\frac{v^2}{2 \; \sigma_v{}^2}\right) \mathrm{d}v \tag{2.33}$$

The calculation can be performed as in Section 2.6 with the only addition of the the power-broadened *width parameter* Γ_ν'. This leads to

$$\begin{aligned} \kappa &= h\nu \; n_0 \; \frac{\alpha_0}{(1 + \frac{2I}{I_s} \frac{\Gamma_\nu}{\Gamma_{\nu,tot}})} \; \frac{1}{\sqrt{2\pi} \; \sigma_\nu} \; \frac{\pi \; \Gamma_\nu'}{2} \; \exp\left(-\frac{(\nu - \nu_0)^2}{2 \; \sigma_\nu{}^2}\right) \\ &= \frac{\kappa_0}{\sqrt{1 + \frac{2I}{I_s} \frac{\Gamma_\nu}{\Gamma_{\nu,tot}}}} \; \exp\left(-\frac{(\nu - \nu_0)^2}{2 \; \sigma_\nu{}^2}\right) \end{aligned} \tag{2.34}$$

and subsequently

$$\kappa = \kappa_0' \; \exp\left(-\frac{(\nu - \nu_0)^2}{2 \; \sigma_\nu{}^2}\right) \; \text{ with } \; \kappa_0' = \frac{\kappa_0}{\sqrt{1 + \frac{2I}{I_s} \frac{\Gamma_\nu}{\Gamma_{\nu,tot}}}} \; . \tag{2.35}$$

2.9   Beer-Lambert Law

As derived before (Eq. 2.35) κ is dependent on the intensity, so solving Equation 2.10 is not an easy task. But in the case of low intensity we can make an assumption that κ is independent from I. The solution of the differential equation is then:

$$I(x) = I_0 \; \mathrm{e}^{-\kappa x} \; . \tag{2.36}$$

This solution is called *Beer-Lambert law* and will be used in Chapter 4 as basis for our evaluation.
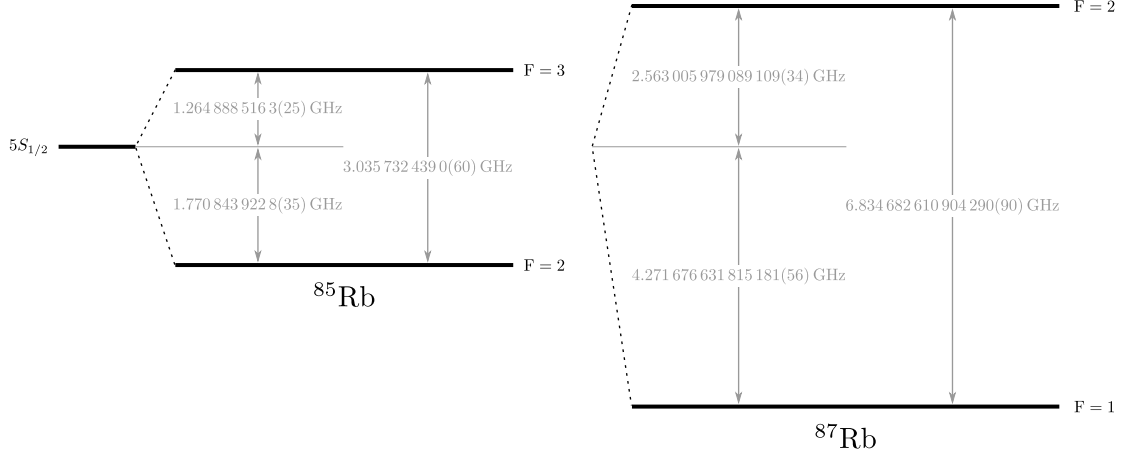
2.10 Real Rb atom D2 line levelscheme

Fig. 2.5 $5^2S_{1/2}$ hyperfine structure of ^{85}Rb and ^{87}Rb.

The transition of interest is, as we have discussed before, the $5^2S_{1/2} \rightarrow 6^2P_{3/2}$ of rubidium. In the cell we use, two isotopes of Rb are present: ^{85}Rb and ^{87}Rb. As we can see both isotopes have the same transition energy, but due to the different spin I (see table: 2.1) the hyperfine energy splitting is different [9]: 3 GHz for ^{85}Rb and 6.8 GHz for ^{87}Rb. This is the reason why we witness four Doppler peaks in our spectrum when performing a spectroscopy (see Fig. 2.6). The different amplitudes between the two isotopes are explained through their abundance in the cell, 72.2 % for ^{85}Rb and 27.8 % for ^{87}Rb. And the cause for the difference among one isotope is that the different hyperfine states, e.g. $F = 2$ and $F = 3$ for ^{85}Rb, have $m_F = 2F + 1$ distinct levels. The thermal energy at 300 K is three orders in magnitude higher than the hyperfine splitting and thus each of the m_F levels are equally populated.
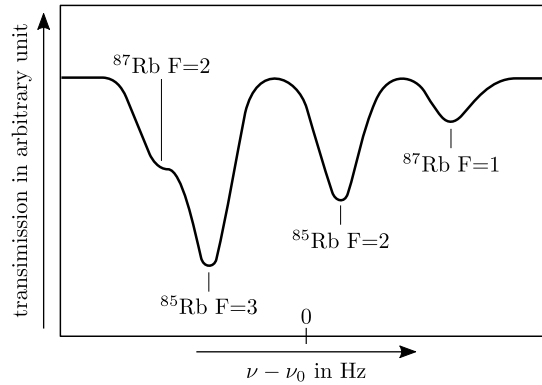
Fig. 2.6 Doppler spectrum of D2 line

2.11   Rubidium data

		Rubidium	
		85	87
Isotope	[1]	85	87
Atomic mass	[u]	84.911794	86.909187
10^{-25}	[kg]	1.40999	1.44316
Abundance	[%]	72.17	27.83
Spin I	[1]	$5/2$	$3/2$
Lifetime $6^2P_{3/2}$	[ns]		112
Lifetime $6^2P_{1/2}$	[ns]		125
Wavelength D1-Line ($6^2P_{1/2} \rightarrow 5^2S_{1/2}$)	[nm]	421.5524	
Wavelength D2-Line ($6^2P_{3/2} \rightarrow 5^2S_{1/2}$)	[nm]	420.1792	
$A_{ki,D1}$, $\Gamma_{\omega,D1}$ @ 421 nm	[s^{-1}]	1.50×10^6	
$A_{ki,D2}$, $\Gamma_{\omega,D2}$ @ 420 nm	[s^{-1}]	1.77×10^6	
Natural linewidth $\Gamma_{\nu,D1}$	[MHz]	0.239	
Natural linewidth $\Gamma_{\nu,D2}$	[MHz]	0.282	

Table 2.1 Properties of rubidium isotopes

Chapter 3

Experiment

3.1 Laser

For all our measurements we used a 420 nm DL (extended cavity laser diode) pro HP laser with a DLC pro controller from Toptica photonics. An optical isolator (OI) is included into the laser and thus the given powers are after OI.

Specifications	
Wavelength:	421.0 nm
Coarse Tuning:	419.5 nm - 422.5 nm
Max. power:	78.0 mW
At diode current:	93 mA
Mode Hop Free Tuning:	79 GHz at 78.5 mA

Table 3.1 Specifications of Toptica DL pro HP 421 nm

The laser has to be tuned to the right wavelength. For that the beam was guided into a fiber and feeded into a wavemeter. The coarse tuning of the laser was done using the mechanical screw which changes the angle of the grating. Then the fine tuning was done playing both on the diode current and the socket temperature on which the laser is mounted. To have a specific output power one would first adjust the diode current, which fines the power and then readjust the temperature.

We characterized the beam profile 50 cm after the beam outlet (see Fig. 3.1), where we could see that the beam had a waist diameter of $\approx 933 \, \mu$m. It should be noted that the beam profile was not perfectly gaussian.
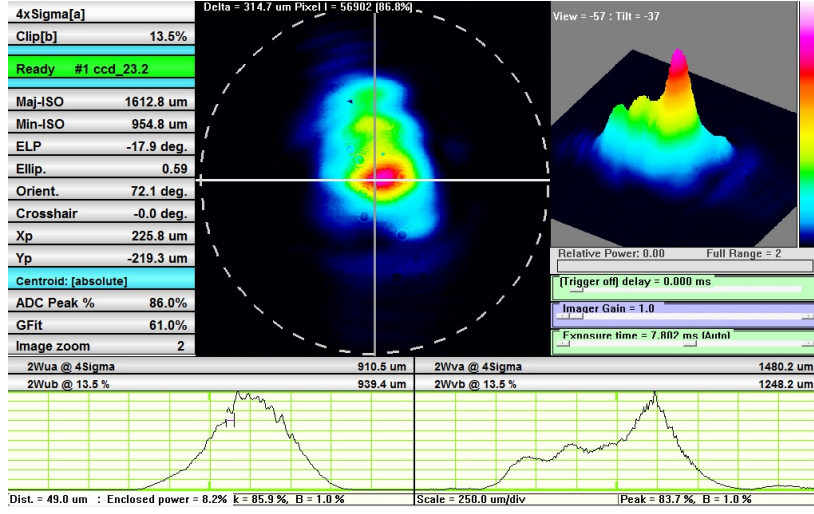
Fig. 3.1 Beam profile after 50 cm

3.2 Setup

Fig. 3.2 Setup mounted on a 60×60cm breadboard.

The laser bench should be placed on the experiment breadboard and thus, we took into account space constraints when designing the beam path (see Fig. 3.2). The whole setup was mounted on a breadboard (60×60cm) and was divided into two parts via a polarization beam splitter (PBS) and a $\lambda/2$ plate. Part of the beam power will be directed to the trap arm. This part was not built, we just placed a beam dump to block the beam, as can be seen in Fig. 3.5. But the occupied area had to be taken into account and we tried to built the spectroscopy setup (second arm) as compact as possible (see Fig. 3.2).
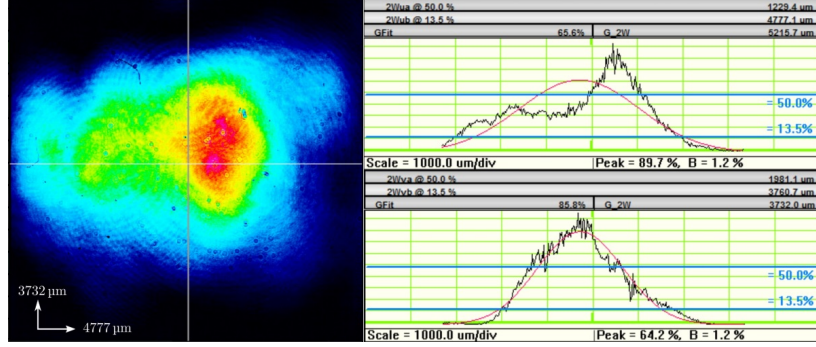
Fig. 3.3 Beam profile after telescope setup.

We want to assume that all atoms receive the same intensity, such that we can use $I = \frac{power}{cross\ section}$. To achieve this, one has to change the beam profile by widening and additionally cropping to the center of the beam. To widen the beam we used a telescope setup after the PBS with two lenses of different focal lengths ($f_1 = 2.5\,\mathrm{cm}$ and $f_2 = 10\,\mathrm{cm}$), which resulted in a beam with a waist diameter of $\approx 3760\,\mathrm{\mu m}$ (see Fig. 3.3). Therefore our magnification is $\frac{3760}{933} = 4 = \frac{10}{2.5}$. Then the beam is cropped using an iris and guided through the cell with two mirrors. The iris aperture was chosen, in order to select the flat intensity. The cell used in the setup is $10\,\mathrm{cm}$ long and containing $^{85}\mathrm{Rb}$ and $^{87}\mathrm{Rb}$ in isotopic concentrations. In order to increase absorption, we heated the rubidium cell with wire coils as seen in Fig. 3.4. We used a wire with a diameter of $0.315\,\mathrm{mm}$ for an higher resistance per unit of length. On the cell are four coils with 35 turns each. The coils have alternating clock- and counter-clockwise windings, such that the generated magnetic fields cancel each other. The heater was operated with $2\,\mathrm{A}$ direct current to produce enough heat such that most of the condensed rubidium changed into the gas phase.
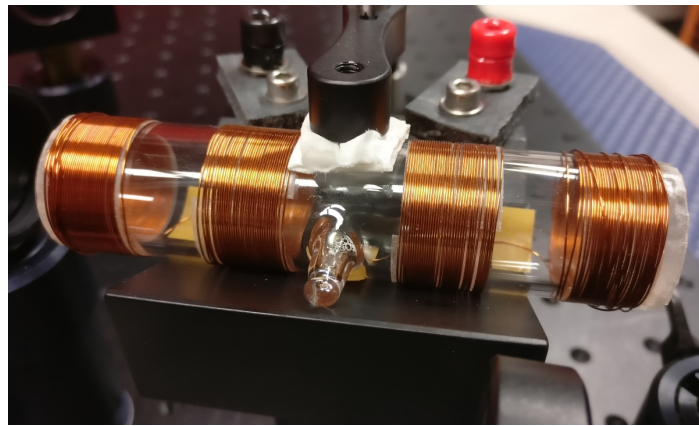
Fig. 3.4 Rubidium cell with applied copper wire coils for heating.

3.3   Laser diameter measurement
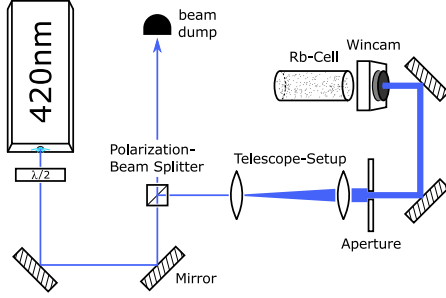
Fig. 3.5 Laser diameter measurement before rubidium cell
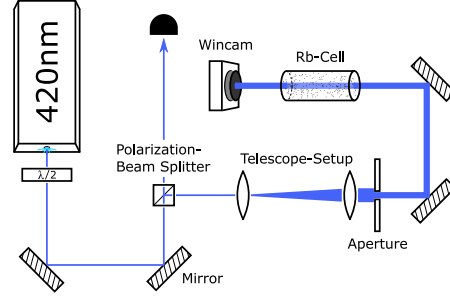
Fig. 3.6 Laser diameter measurement after rubidium cell

In order to calculate the laser intensity one needs to measure the beam power and the beam cross section or rather the beam diameter. With a beam profiler (in our case a WinCamD) a measurement is performed in front and after the cell to measure and characterize the beam profile and check if the beam is collimated after the widening (see Fig. 3.5 and 3.6). The beam waist diameter calculated by the WinCamD application (see Fig. 3.10) under the assumption of a gaussian beam is not correct. We will instead use a flat hat model for the evaluation and take the diameter where the power drops to half of the maximum power. It should be noted that the power is not constant over the whole beam profile, but shows 30% of fluctuations. We can then use the mean where the edge of the beam maximum is determined by hand. This leads to an uncertainty of $\pm 100\,\mu\mathrm{m}$ per measurement. To obtain the equivalent flat hat intensity one has to integrate over the plot from limit to limit and divide by the interval (see Fig. 3.8). The diameter of the beam is defined by its FWHM, this would be half the mean intensity as seen in Fig. 3.9. The estimated beam diameter before the cell calculated out of the x- and y-axis slice is $(1608 \pm 70)\,\mu\mathrm{m}$ and $(1649 \pm 70)\,\mu\mathrm{m}$ after the cell. Therefore the mean diameter is $(1628 \pm 50)\,\mu\mathrm{m}$ which leads to an estimated cross section of $(2.083 \pm 0.128) \times 10^{-6}\,\mathrm{m}^2$.
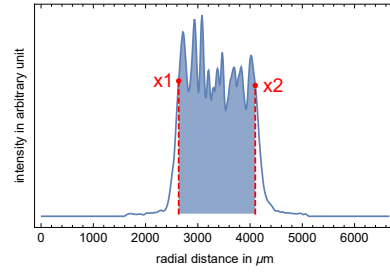
Fig. 3.7 By hand estimated beam limits.
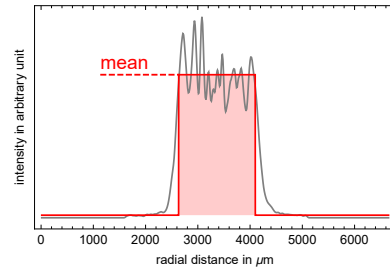

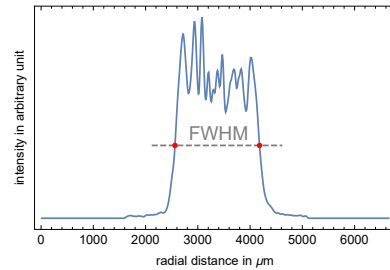**Fig. 3.8** Equivalent flat hat beam.

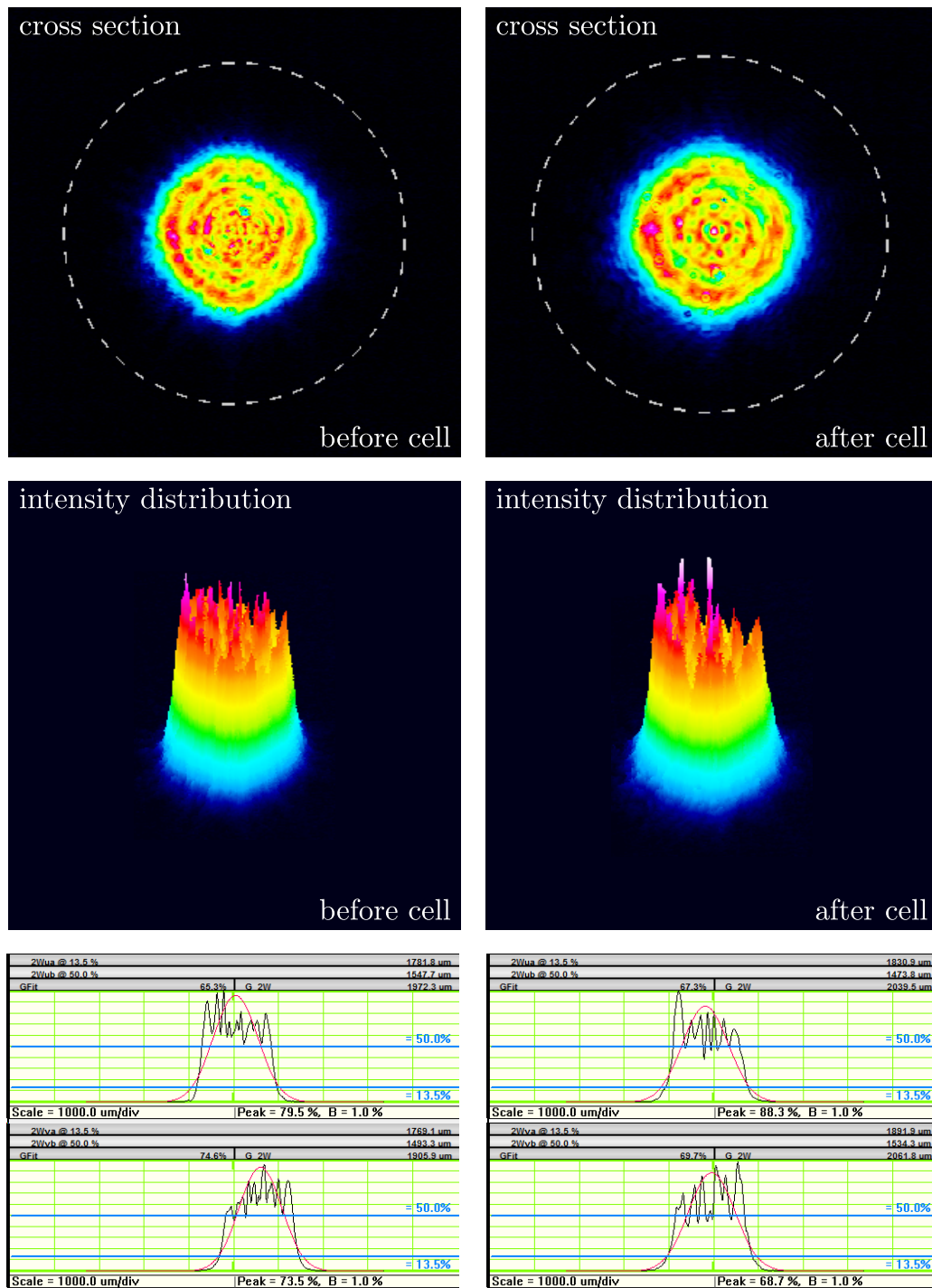**Fig. 3.9** FWHM defines the estimated diameter.

Fig. 3.10 Cross section, intensity distribution and x- and y-axes slices through beam center before and after cell transit.

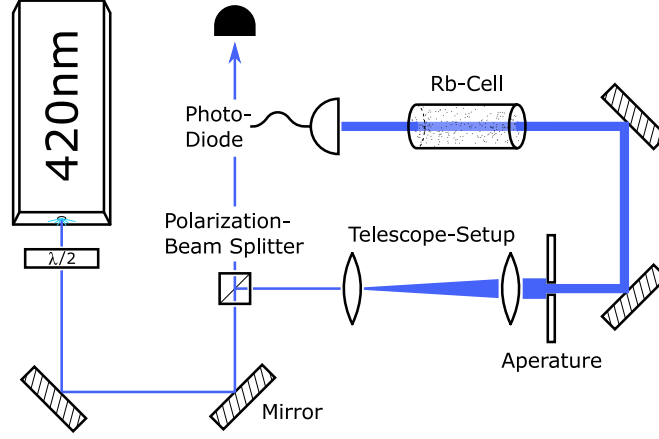## 3.4   Absorption spectroscopy

Fig. 3.11 Setup for an absorption spectroscopy.

We want to measure the intensity after the cell as a function of the initial intensity I_0. The transmitted intensity depends on the detuning as shown in formula 2.35.

We will thus scan the laser frequency across the atomic resonances and for each input power record the signal using a photodiode (PD) (see Fig. 3.11) connected to a Teledyne Lecroy HDO6000A a digital storage oscilloscope. The PD records a signal proportional to the intensity only for a given range of power, so we made sure that we where using the PD in the linear range (see Fig. 3.12). The gain of the PD was adjusted in order to not saturate the signal, but to have the widest possible dynamics to obtain the best signal to noise ratio. To change the input power, we turned the $\lambda/2$ plate before the polarizing beam splitter (PBS) and measured it before every spectroscopy. It should be noted that changes of the sensor position in between measurements and variation of the remaining ambient light lead to an increasing uncertainty at lower beam power. We account for 10 % uncertainty below
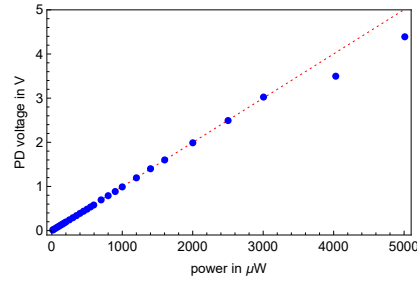

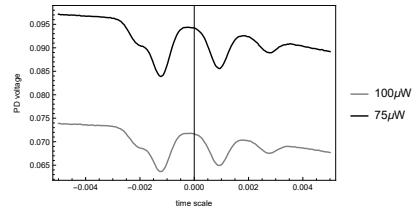**Fig. 3.12** Maximum PD voltage taken out of atomic resonance over power measured before the cell to ensure PD linearity; measurements at $4000\,\mu\text{W}$ and $5000\,\mu\text{W}$ will be excluded.

Fig. 3.13 Absorption spectra at $75\,\mu\text{W}$ and $100\,\mu\text{W}$.

$100\,\mu\text{W}$, 8 % below $250\,\mu\text{W}$, 6 % below $1000\,\mu\text{W}$ and 3 % above.
Before the spectroscopy itself, after the power was measured, the heating system, due to

its noise generating magnetic field, and all lights besides the measuring equipment were turned off. The spectroscopy was performed by scanning the laser wavelength using the piezo scanning option of the DL pro controller. We centered the scan range for all the measurements using the controller and the oscilloscope. For each input power we recorded the spectra and saved it onto a USB stick for further data analysis. We followed a logarithmic progression for the power increments from $13\,\mu W$ to $5000\,\mu W$. Two examples of the recorded spectrum are shown in Fig. 3.13. The choice of the power together with the beam cross section, should enable to probe intensity range from below to above I_s.

In the next chapter we will discuss the analysis of the gathered data.

Chapter 4

Evaluation

The scanning span we used was more than the $6.86\,\mathrm{GHz}$ of the hyperfine splitting of ^{87}Rb. We thus observe four absorption dips due to ^{87}Rb $F = 1$ and $F = 2$ and ^{85}Rb $F = 2$ and $F = 3$. In the data analysis, we treated each of the dips as a two-level atom, using the theory described in Chapter 2.

We are interested in determining I_s, which is included in κ_0' (see Eq. 2.35). We will use the Beer-Lambert law $I(x) = I_0\,\mathrm{e}^{-\kappa x}$, which leads on resonance to

$$I(x, \nu_0) = I_0\,\mathrm{e}^{-\kappa_0' x} \ . \tag{4.1}$$

Which gives us an expression for κ_0'

$$\kappa_0' = -\frac{1}{L}\,\ln\left(\frac{I(L, \nu_0)}{I_0}\right) \tag{4.2}$$

where L is the cell length.

Thus, one needs to extract from the absorption spectroscopy dips $I(L, \nu_0)$ and I_0. We measured $I(L, \nu_0, I_0)$ for different values of I_0 and computed the experimental κ_0. We will then fit the theory formula 2.35 using I_s and T as free parameters to extract them for the four "atoms".

4.1 Model fit on absorption spectra
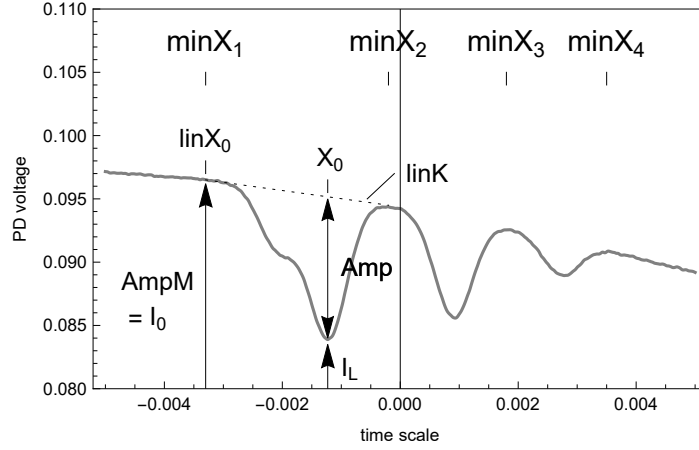
Fig. 4.1 Definition of all model parameters for the ^{85}Rb $F = 3$ line.

The whole data analysis and parameter fitting has been made using mathematica. To narrow down the range for our fits of the different lines we defined four constants $minX_1$ to $minX_4$ which mark the beginning or the end of one dip. As can be seen in Equation 2.35 all our spectra are based on a gaussian model, but due to the short separation of the ^{87}Rb $F = 2$ and ^{85}Rb $F = 3$ line we have also an overlapping double gaussian. To reduce mode hopping the laser adjusted the beam power during the scan and therefore our spectra have a linear decrease in power. Our fitting models are based on a double and two single gaussians. For the explanation of all the parameters we will use the ^{85}Rb $F = 3$ line as an example (see Fig. 4.1).

$$Gauss1 = AmpM - Amp \cdot Exp\left(-\frac{(x - x_0)^2}{2\,\sigma^2}\right) + linK(x - linX_0) \tag{4.3}$$

$$Gauss2 = AmpM - Amp1 \cdot Exp\left(-\frac{(x - x_1)^2}{2\,\sigma_1^2}\right) - Amp2 \cdot Exp\left(-\frac{(x - x_2)^2}{2\,\sigma_2^2}\right)$$
$$+ linK(x - linX_0)\,, \tag{4.4}$$

where *AmpM* is the maximum power without absorption, *Amp* is the amplitude of the absorption, x_0 is the center of the absorption line, σ is the standard deviation of the gaussian, $linK$ is the slope of the power decrease and $linX_0$ is the beginning of the gaussian. In case of the double gaussian the different parameters of the gaussians are labeled with the indices "1" and "2".

With these two models all the spectra where fitted and the obtained parameters where saved into a single table for further analysis. The error bars of the fits where saved into a separate

table, which we will use for the uncertainties of the absorption coefficient. One example of the fitted models is shown in Fig. 4.2. All the info we want is contained in *AmpM* and *Amp*.
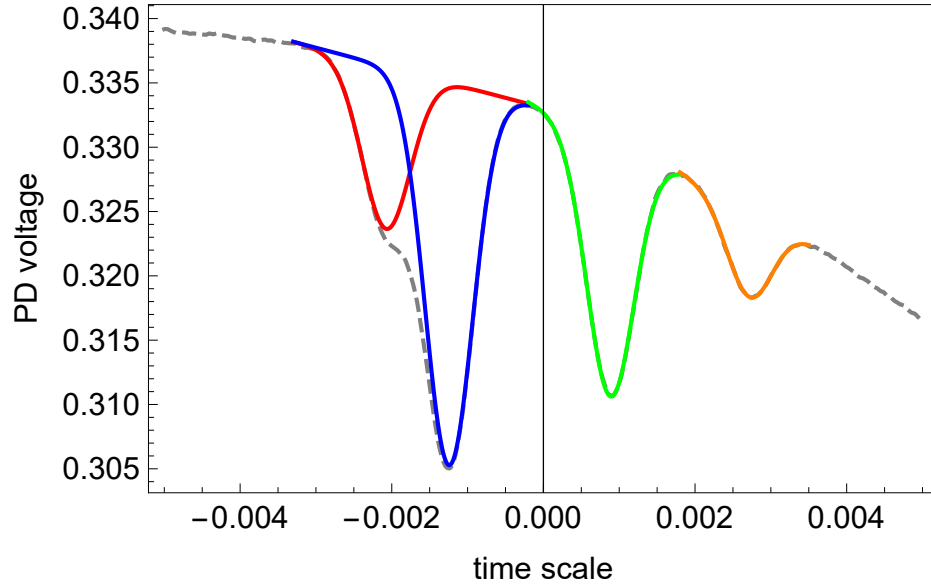

Fig. 4.2 Absorption spectrum at $350\,\mu\text{W}$ with the fitted absorption lines.

4.2   Power extraction

To link *AmpM* to the power measured with the powermeter, we need to take into account that the power measured before the cell corresponds to the mean value over the scanning range. For that reason we calculated the power at each transition position, assuming a linear decline and considering that the mean value lies in the middle of the minimum and maximum power (see Fig. 4.3). We applied these corrections for all our data sets. An example of the extracted powers can be found in Table. 4.1. The error bars come from the powermeter uncertainties.
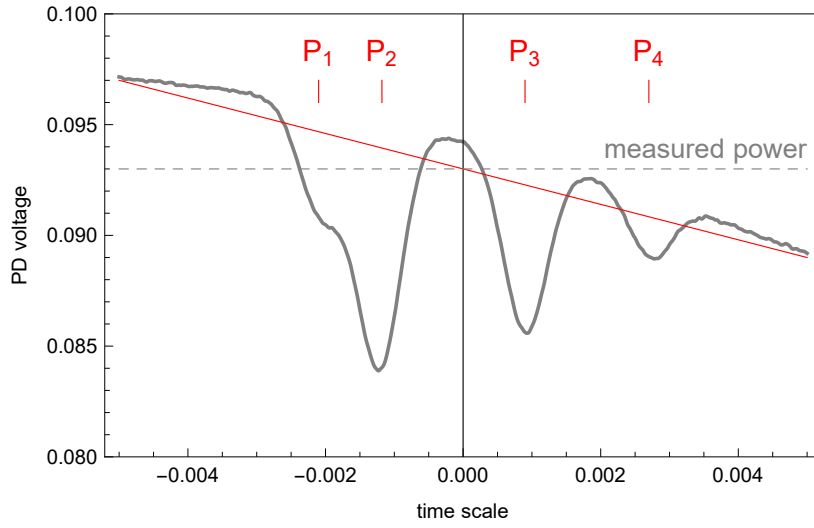
Fig. 4.3   Linear approximation on power decrease

measured power: $350\,\mu\mathrm{W}$

line	power [µW]	uncertainty [µW]
^{87}Rb $F = 2$	355	21
^{85}Rb $F = 3$	353	21
^{85}Rb $F = 2$	347	20
^{87}Rb $F = 1$	343	20

Table 4.1   Power correction for $350\,\mu\mathrm{W}$ measurement.

4.3 Measured absorption coefficient

To determine the absorption coefficient, we have to calculate the intensity for all transitions and measurements. For this we will use the estimated cross section of Section 3.3 and the flat hat model $I = \frac{power}{cross\ section}$. The error bars are based on the uncertainties of the power measurement given in Section 3.4. As an example the calculated intensities for the $350\,\mu W$ measurement can be found in Table 4.2.

calculated intensity at $350\,\mu W$: $168\,W\,m^{-2}$		
line	intensity $[W\,m^{-2}]$	uncertainty $[W\,m^{-2}]$
$^{87}Rb\ F = 2$	170	14
$^{85}Rb\ F = 3$	169	14
$^{85}Rb\ F = 2$	167	14
$^{87}Rb\ F = 1$	165	14

Table 4.2 Corresponding intensities to the power correction of the $350\,\mu W$ measurement.

With Equation 4.2 and the length of the rubidium cell ($L = 0.1\,m$) one can now determine κ_0' for all lines and measurements. As we can see in Fig. 4.1 I_0 corresponds to $AmpM$ and $I(L, \nu_0)$ to $AmpM - Amp$. It should be noted that we make an error on the assumption of $AmpM \cong I_0$, because of the linear decrease of amplitude/power over ν (see Fig. 4.3). We can limit the maximum error to $3\,\%$, due to the fact that the maximum relative amplitude deviation over the whole spectrum is on average $6\,\%$. This will be taken into account for the calculation of κ. The uncertainties for the different absorption coefficients are based on the uncertainties of the gaussian fit of the spectrum, which where extracted in Section 4.1. An example for the measured absorption coefficient is given in Table. 4.3.

absorption coefficients at $350\,\mu W$		
line	$\kappa\ [m^{-1}]$	uncertainty $[m^{-1}]$
$^{87}Rb\ F = 2$	0.38	0.17×10^{-3}
$^{85}Rb\ F = 3$	0.92	0.19×10^{-3}
$^{85}Rb\ F = 2$	0.62	0.20×10^{-3}
$^{87}Rb\ F = 1$	0.21	0.13×10^{-3}

Table 4.3 Calculated absorption coefficients for $350\,\mu W$ measurement.

The absorption coefficients calculated from our spectroscopy will then be fitted to the theoretical ones.

4.4   Saturation intensity determination

To account for isotope proportions and hyperfine level populations (see Sec. 2.10), each of the absorption coefficient models for our fit will be balanced, because it changes the atom density n_0. In detail, we have a vapor constituted of the two atoms in two states each and their abundance depend on isotope concentration and on atom m_F level population. So we have

$$n_{0,tot} = n_{0,^{87}Rb\ F=2} + n_{0,^{85}Rb\ F=3} + n_{0,^{85}Rb\ F=2} + n_{0,^{87}Rb\ F=1} \ . \tag{4.5}$$

Where for each atom n_0 is replaced by $n_{0,tot} \times ratio_X$ (see Table. 4.4)

κ model adaptation			
line	isotope abundance	hyperfine levels	$ratio_X$
^{87}Rb $F = 2$	0.2784	5/8	0.174
^{85}Rb $F = 3$	0.7216	7/12	0.421
^{85}Rb $F = 2$	0.7216	5/12	0.301
^{87}Rb $F = 1$	0.2784	3/8	0.104
			1.000

Table 4.4 Atomic density ratios of the different isotopes and hyperfine lines

This leads to our model based on Equation 2.35

$$\kappa'_{0,X} = n_{0,tot}\ ratio_X\ \frac{\pi^2 \Gamma_\nu{}^2}{I_s}\ h\ \nu_0\ \frac{c}{\nu_0}\ \sqrt{\frac{m_X}{2\pi\ k_B T}}\ \frac{1}{\sqrt{1 + \frac{2I}{I_s}\frac{\Gamma_\nu}{\Gamma_{\nu,tot}}}}\ , \tag{4.6}$$

where X stands for the different lines. The total atom density $n_{0,tot}$ can be extracted out of the vapor-pressure model [10]:

$$\log_{10} P_V = 4.312 - \frac{4040}{T}\ , \tag{4.7}$$

where P_V is the pressure in atmospheres and the ideal gas law, such that

$$n_{0,tot} = \frac{1}{k_B T}\ 10^{9.318 - \frac{4040}{T}}\ . \tag{4.8}$$

We use Mathematica to fit our data and because we want to include the obtained error bars for the fit, we are restricted to a NonlinearModelFit. Moreover it is only possible to have error bars on the y-axis of your data, which will be incorporated via a weight on every data point. For this reason we had to choose the measurement with the larger error bars as our

y-axis. We can see in our calculation that the error bars on κ are two orders of magnitude smaller than the errors bars on the calculated intensity (see Tables 4.2 and 4.3). However our models are κ depending on I. For that reason we have to exchange x- and y-axis of the used data sets and invert our model so we get $I(\kappa)$ instead of $\kappa(I)$.

To extract κ of our measurements we used the Beer-Lambert law, which assumes that κ is independent from I. This assumption is only true for intensities below I_s. Therefore we have to limit our measurement data where the initial intensity is below $I_s = 126\,\mathrm{W\,m^{-2}}$, which is the theoretical one (see Fig. 4.4). Therefore we get following values and corresponding error bars for I_s and temperature T for every absorption line extracted (see Table 4.5):

saturation intensity and temperature				
line	I_s [W m^{-2}]	uncertainty [W m^{-2}]	T [K]	uncertainty [K]
^{87}Rb $F=2$	45.6	1.8	336.9	0.4
^{85}Rb $F=3$	51.7	2.5	338.2	0.5
^{85}Rb $F=2$	37.2	2.6	334.5	0.6
^{87}Rb $F=1$	30.7	3.3	332.3	0.9
mean value	41.3		335.5	

Table 4.5 Fitted values of I_s and temperature.
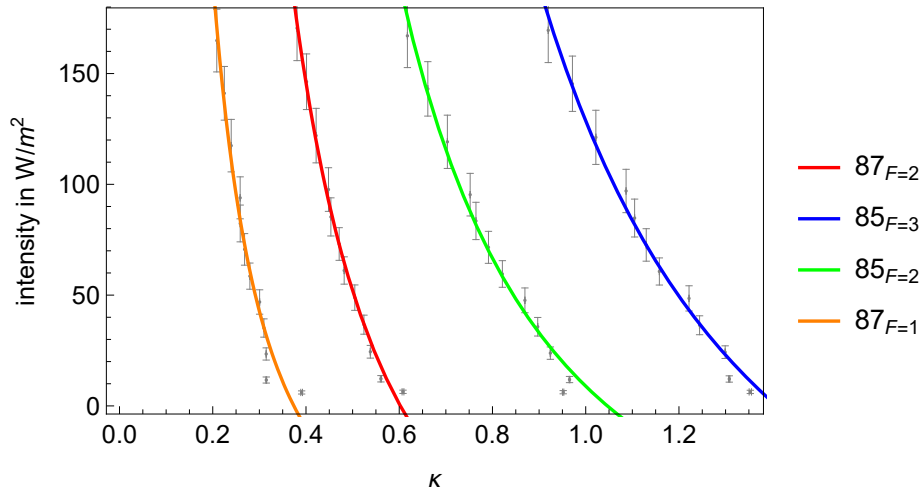
Fig. 4.4 Plot of the four inverted absorption coefficients with corresponding error bars

Conclusion

The values of I_s for the different fits are quiet scattered. Normally one should measure the same value for both isotopes and independently of the internal state. This is an indication that we probably underestimated error bars. For example, we considered a scan over the line to be linear in frequency but it is probably a sinusoidal modulation and we did not take that into account in your fits. Additionally the obtained value is much smaller than the theoretical value $(126\,\mathrm{W\,m^{-2}})$. This is not what we would expect. Due to deficiencies, like a finite transmission of the cell windows, normally one has to send more power than in theory. The discrepancy of a factor of 4 between the measurement and the theory can still be understood by different misestimates during the measurement and data processing.

One reason would be that the Beer-Lambert law was not valid, because our beam intensity was to high. This was checked by selecting only measurements with lower intensity, but it only leads to a $10\,\%$ improvement. Another reason for the deviation could be the use of the wrong polarization for the beam. Instead of π-polarization it should be σ_+ or σ_- to drive a closed transition. But the most prominent cause for our low saturation intensity is by far the rough shape of our beam profile, which leads to an inaccurate determination of the input intensity. Due to the power fluctuations of $30\,\%$ over the beam diameter, part of the atoms would saturate before the rest. One could now calculate a more complicated intensity profile and repeat the analysis. An overall increase in intensity would improve I_s in direct proportions.

In conclusion, in this thesis we have studied the possibility to use the $5S_{1/2}$ to $6P_{3/2}$ transition to create a dipole trap for atoms close to a microresonator surface. We have then reported on the implementation of a new laser bench used to realize this dipole trap. And in order to confirm that the order of magnitude of the transition strength $\Gamma_{6P_{3/2}}$ was indeed correct, we performed a spectroscopy measurement, leading to the evaluation of I_s for this transition. This spectroscopy could also be used to lock the laser on an atomic resonance, which will be needed, since the estimated detuning needed for the trap to be deep enough is to small to let the laser freerunning.

References

[1] L.-M. Duan and H. J. Kimble. Scalable photonic quantum computation through cavity-assisted interactions. *Phys. Rev. Lett.*, 92:127902, Mar 2004.

[2] J. D. Thompson, T. G. Tiecke, N. P. de Leon, J. Feist, A. V. Akimov, M. Gullans, A. S. Zibrov, V. Vuletić, and M. D. Lukin. Coupling a single trapped atom to a nanoscale optical cavity. *Science*, 340(6137):1202–1205, 2013.

[3] R. Grimm, M. Weidemüller, and Y. B. Ovchinnikov. Optical Dipole Traps for Neutral Atoms. *Advances in Atomic Molecular and Optical Physics*, 42:95–170, 2000.

[4] Matthias Schulz. *Tightly confined atoms in optical dipole traps.* PhD thesis, Leopold-Franzens-Universität Innsbruck, 2002.

[5] Bindiya Arora and B. K. Sahoo. van der waals coefficients for alkali-metal atoms in material media. *Phys. Rev. A*, 89:022511, Feb 2014.

[6] Danny O'shea. *Cavity QED experiments with a whispering-gallery-mode bottle resonator.* PhD thesis, Vienna University of Technology, ???

[7] Department of Physics. Saturated absorption spectroscopy. *University of Florida*, 2001.

[8] Department of Physics. Appendix - saturated absorption spectroscopy. *University of Florida*, 2001.

[9] J. Reader A. Kramida, Yu. Ralchenko and NIST ASD Team (2015). NIST atomic spectra database (ver. 5.3). *National Institute of Standards and Technology*, 2015.

[10] C. B. Alcock, V. P. Itkin, and M. K. Horrigan. Vapour pressure equations for the metallic elements: 298–2500k. *Canadian Metallurgical Quarterly*, 23(3):309–313, 1984.

List of figures

List of tables